Dual-wavelength switchable single-mode lasing from a lanthanide-doped resonator

Yunkai Wu
Harbin Institute of Technology
Xian Chen
Shenzhen University
Limin Jin
Harbin Institute of Technology https://orcid.org/0000-0002-2697-8811
Xiangzhe Ai
Shenzhen University
Shumin Xiao
Harbin Institute of Technology https://orcid.org/0000-0002-0751-9556
Xiaoli Yang
Harbin Institute of Technology, Shenzhen
Qinghai Song (qinghai.song@hit.edu.cn)
Harbin Institute of Technology https://orcid.org/0000-0003-1048-411X

Article

Keywords: upconversion material, single-mode lasing, unidirectional, microlaser switch

Posted Date: April 21st, 2021

DOI: https://doi.org/10.21203/rs.3.rs-418011/v1

Version of Record: A version of this preprint was published at Nature Communications on April 1st, 2022.
See the published version at https://doi.org/10.1038/s41467-022-29435-w.

Abstract

Multi-wavelength lasing, with dynamic switching functionality, high spectral purity and contrast, plays an essential role in photonic devices. Lanthanide(Ln^{3+})-doped upconversion nanocrystals(UCNCs) featured with plentiful energy levels act as ideal candidates for the gain medium. However, it remains a daunting challenge to develop a tunable Ln^{3+}-based single-mode laser across a wide wavelength range due to the absence of an appropriate mode-selection mechanism. Here, we have demonstrated the first active control of unidirectional single-mode lasing with switchable wavelength spanning beyond a record range (~ 300 nm). This is accomplished through the integration of two size-mismatched coupled microdisks cavity and inversely designed dual-mode UCNCs incorporated with selective sensitizer-pair and activator ions. By asymmetric pumping, a reversible and crosstalk-free ultraviolet-to-red single-mode operation were formed respectively from such UCNCs-based system through changing the pumping wavelengths from 980 nm to 808 nm. The results enlighten the rational design of luminescent materials and microcavity. With remarkable doping flexibility, our approach would pave an avenue to a class of UCNCs-based photonic devices for on-chip optical filter, switch, sensor and other devices.

Introduction

Multi-wavelength laser from one single luminescent material capable of emitting wavelengths over a wide spectrum range fulfills a subject of great applications, including general lighting, high-throughput sensing, multicolour imaging, laser display, high-level security, on-chip recording and communication[1–3]. The ultimate form of such laser lies in a type of crosstalk-free monochromatic single-mode operation with high contrast and reversibility in a wide tuning range. In fact, lanthanide (Ln^{3+})-doped upconversion nanocrystals (UCNCs), owing to their characterized multicolour emissions spanning from ultraviolet (UV) to near infrared (NIR)[4–5], shows remarkable potential as the gain medium.

Hereunto, considerable efforts have been devoted to engineer the luminescence profile of UCNCs at will by taking advantage of remote manipulation or chemical strategies. Upconversion processes are primarily dependent on Ln^{3+}-doped materials featuring with highly shielded $4f^N$ electrons, which give rise to intriguing optical properties such as large anti-strokes shifts, narrow absorption/emission bands, long radiative lifetime, metastable energy levels, and so on[4–5]. Such efficient tailoring of UC emission refers to selectively enhancement or suppression of some specific emitting peak through manipulating multiphoton upconverting processes. Generally, colour-tunable emission can be realized through precise control of doping concentration and composition[6–9]. For instance, Wang et al have reported colour management in visible-NIR spectral range from a Yb^{3+}-Er^{3+}-Tm^{3+} tri-doped $NaYF_4$ host upon irradiation with light of a single wavelength[6]. UC emission can also be expanded to other Ln^{3+} ions without long-lived intermediary energy states through feasible Gd^{3+}/Er^{3+}/Tb^{3+}-mediated energy migration[7–9]. In essence, these methods, which were experimentally realized through the reconstruction of UCNCs, heavily rely on the stringent control over a combination of parameters involving crystal composition, structure,

size, shape, and surface ligand [4–5, 10–11]. Clearly, such gradient doping and manipulation at the nanoscale are time-consuming, and sometimes the choice is an experimental accident.

An explosive amount of research has witnessed the deep investigation of *in situ* light-guided upconversion. In 2010, Chen group proposed dual-mode luminescence from $NaGdF_4$:Yb/Tm@ $NaGdF_4$:Eu nanoparticles while being illuminated by 980 nm and 273 nm light source respectively[12]. Other nanostructures benefiting from co-doped sensitizer-pair were exemplified one after another[13–14]. Later, dynamic full-colour tuning was achieved from a fixed UCNCs by adjusting the pulse width of the pumping laser[15]. The emitting range of UCNCs was further expanded to deep UV region, a 5-photon upconverted lasing at 311 nm of Gd^{3+} ions, through sequential pulse pumping[16]. In the parallel studies, the demonstration of power-dependent fluorescence was conducted by Zhao group and Zhang group, respectively[17–18]. Similarly, thanks to their different luminescent lifetime, Ln^{3+}-related time-dependent emission can be found at characteristic lifetime observation windows[19]. Apart from that, stimuli-dependent UC luminescent materials in response to temperature, pH, electric field, magnetic field, and mechanical force have emerged as interesting alternatives for the generation of spectral management[20–28]. Note that, an irreversible phase change of UC materials would happen above 400°C, responsible for the enhanced luminescence [21]. Attempts tend to focus on the generation of featured photoswitch with both sharp contrast and steep on/off switch, but achieving this goal remains a tremendous challenge.

Herein, we demonstrate that a novel UCNCs-doped size-mismatched photonic molecule (PM) structure, evoking constructive Vernier effect in the resonance between excited and unexcited constituent microdisk upon asymmetric pumping, gives rise to excellent unidirectional single-mode lasing with output of choice. This PM in submillimeter scale was made in silicon-on-insulator with 2 μm buried oxide with CMOS-compatible photolithography technique, providing a smart and robust design to construct a mass-manufacturable coupled cavity without sophisticated manipulation of two adjacent microdisks in nanoscale precision[29]. By harnessing Yb^{3+}-Nd^{3+} co-doped UCNCs as the gain medium, dynamic switch of resulting supermodes with an ultralarge shift up to 300 nm (Table 1 in supporting information) is realized by simply changing NIR excitation wavelengths. On this basis, chemical flexibility of UCNCs, as well as tailorable gain region, would advance the utility of this strategy that allows the generation of unidirectional single-mode laser action at arbitrary design wavelength ranging from ultraviolet to NIR regime.

Results

The working mechanism of our proposed UCNCs-based microlaser is schematically displayed in Fig. 1, which integrates two key advances involving gain material and cavity design to endow dynamically tunable single-mode laser. In this design, light manipulation at nanoscale (Fig. 1a) is achieved through dispatching different Ln^{3+} ions into separated layers of multishelled UCNCs, which thus enable two distinct upconverting processes under the excitation of λ_1 and λ_2 lasers, respectively. Upon pumping at

different wavelengths, the integration of those UCNCs and microdisk resonator (Fig. 1b) from patterned substrate[30] would lead to two groups of multicolour lasing emission through the formation of whispering gallery modes (WGMs). Such an arrangement usually suffers from inherently isotropic output as well as multiple modes feature arising from simple microdisk laser. According to the following equation[16, 30]:

$$FSR = \lambda_0^2 / n_{eff} L \quad (1)$$

where FSR is the free spectral range, λ_0 is the wavelength of resonant peak, n_{eff} is the group refractive index, and L is the optical length, single-mode operation could be achieved by decreasing the size of cavity down to several or a dozen of microns[16, 30]. However, this strategy is quite limited since it usually gives rise to a highly increased lasing threshold while the multicolour output problem cannot be effectively addressed. To overcome these obstacles, the UCNCs-based size-mismatched PM structure with the cavity size at the submillimeter scale can be exploited to attain single-mode laser under asymmetric excitation (Fig. 1c). Once PM laser is established by withholding the excitation from one of two tangent microdisks, a single-mode laser emerges from two coupled microdisks cavity, a stark contrast to microdisk lasers. In this regard, other competing modes would be highly suppressed. Most importantly, through external excitation manipulation, this on-chip PM device offers robust dynamic mode-switching functionality without the need for any other intricate components.

As a proof of concept, $NaGdF_4$:Yb/Nd@$NaGdF_4$:Yb/Ho@$NaYF_4$:Ca@$NaYbF_4$:Tm@$NaYF_4$:Ca core-multishelled UCNCs were synthesized *via* a modified literature procedure [16]. Generally, $NaGdF_4$:Yb/Nd core nanocrystals with a diameter of ~ 16 nm were firstly prepared followed by successive deposition of four epitaxial shells of $NaLnF_4$ (Ln = Gd, Yb, Ho, Tm, Y). Note that, the $NaYF_4$:Ca inner layer with a thickness of 5 nm is used to prohibit the $Nd^{3+} \rightarrow Yb^{3+} \rightarrow Tm^{3+}$ energy transferring path (Figure S2 and Figure S3) under 808 nm excitation, while the outmost layer of $NaYF_4$:Ca is employed to suppress surface quenching and protect upconverting processes. The Yb^{3+} clusters were conducted in the neighboring layer to mediate the energy transfer from Nd^{3+} to Ho^{3+} ions and avoid concentration quenching effect. The successful synthesis of the core-multishelled UCNCs was inferred from the results of transmission electron microscopy (TEM, Fig. 2a and Figure S1), X-ray powder diffraction (Figure S4) and photoluminescence (PL, dotted lines in Fig. 2e) results. It is interrogated that the monodispersed UCNCs, with uniform size at ~ 40 nm in diameter, reveal a single-crystalline nature with the Bragg diffraction lines expected for the hexagonal-form $NaYF_4$ (JCPDS #16–0334). As plotted in Fig. 2b, high-resolution TEM image and the Fourier transform diffraction pattern permit resolution of lattice fringes of {100} with a *d*-spacing of 0.52 nm, which matches with that of *β*-$NaYF_4$ [16, 30]. For optical characterization, the UCNCs solution was measured under the excitation of continue-wave (CW) NIR laser. The Nd^{3+}/Yb^{3+} sensitizer-pair clearly leads to two groups of characteristic peaks of Ho^{3+} and Tm^{3+} ions while being optically pumped at the wavelengths of 808 nm (Fig. 2e, top PL) and 980 nm (down PL), respectively. Typically, for 808 nm pumped case, the excitation energy would be harvested by Nd^{3+} ions incorporated in the core layer, then migrating to Ho^{3+} ions in the first shell layer through Yb-sublattice,

while Tm^{3+} ions would dominantly exhaust the excitation energy collected by highly doped Yb^{3+} ions under conditions of 980 nm excitation. As shown in Fig. 2e, these emitting peaks can be assigned to $^5F_3 \rightarrow {}^5I_8$ (487 nm), $^5S_2 \rightarrow {}^5I_8$ (542 nm), and $^5F_5 \rightarrow {}^5I_8$ (646 nm) transition of Ho^{3+} ions, and $^1I_6 \rightarrow {}^3F_4$ (346 nm), $^1D_2 \rightarrow {}^3H_6$ and $^3F_4$ (362 and 451 nm), and $^1G_4 \rightarrow {}^3H_6$ and $^3F_4$ (476 and 648 nm) transition of Tm^{3+} ions, respectively. The weak peak at 542 nm and 648 nm under 980 nm pumping may arise from $Yb^{3+} \rightarrow Ho^{3+}$ upconversion process. This unique behaviour of such UCNCs allows it to be a promising candidate for constructing dynamic switchable microlaser.

We subsequently fabricated UCNCs-based microdisk array by simply spin-coating a mixture of UCNCs and silica resin (6.5 wt%) onto the preformed SiO_2 substrate [30]. Figure 2c and 2d show the scanning electron microscopy (SEM) images of UCNCs-on-SiO_2 microdisk array and an isolated one (d = ~ 100 μm, t = ~ 300 nm), respectively. The UCNCs-based microdisk well inherits the pattern of underneath SiO_2 pillar. For its laser characterization, a NIR pulsed laser (808/980 nm, pulsewidth 6 ns, repetition rate 10 Hz, Φ8 mm) is focused onto the top surface of the microdisk, with the emission light from the boundary of the cavity being collected by an optical fiber coupled to a monochromator. Figure S5 and S6 summarize the lasing actions in UCNCs-based microdisk under NIR excitation. For instance, we observed that several periodic sharp peaks centered at 345.8 nm emerge from the broad emission band once above the transparent threshold (i.e., P_a = 47.02 mJ cm^{-2}, as reflected by the first kink value in Figure S5c), and then quickly dominate the emission spectra as the increase of pumping fluences. This experimental FSR reads as ~ 0.24 nm, which matches the calculated one from the formula (1) (i.e., n_{eff}, ~ 1.58, and L are the group refractive index and the perimeter of UCNCs-based microdisk) [30]. Concurrently, the transition from spontaneous emission through amplification to lasing oscillation, as reflected by three regions with distinct slopes, is clearly visible from the corresponding light-light curves[16, 30]. Both this power-dependent behaviour and the well-defined mode spacing values confirm the lasing action along WGMs. Similar laser behaviour has also been observed in other characteristic peaks (Sect. 3 in Supporting Information) except for the resonance peaks at 542 nm and 648 nm under the excitation of 980 nm laser, since there is no sufficient gain to support efficient population inversion. As anticipated, the profile of the observed multicolour WGMs lasers exhibit pronounced differences while being excited by 808 nm and 980 nm lasers respectively.

WGMs lasing actions derived from Ln^{3+}-doped materials have been well understood in many similar systems [16, 30–32]. Notably, single-mode laser can be realized in precisely regulated resonators with the diameter down to 4 μm or 20 μm [16, 32]. Moreover, an enhanced 290 nm (i.e., $^1I_6 \rightarrow {}^3H_6$ of Tm^{3+}) lasing was reported in a microdisk laser through suppressing competitive emission at 345 nm (i.e., $^1I_6 \rightarrow {}^3F_4$ of Tm^{3+}) *via* keeping the thickness of UCNCs-based microdisk at a “cutoff” value (around 130–140 nm)[30]. However, other characteristic peaks including 362 nm, 451 nm, 476 nm, 545 nm and 648 nm of Tm^{3+} ions can hardly be simultaneously quenched at a given cutoff thickness or through other chemical approaches. Consequently, the presence of such multicolour, multimode and isotropic output feature in

Ln^{3+}-based microdisk lasers leads to temporal and spatial fluctuations of the light source[33], thus is destructive to spectral purity and beam quality.

For precise mode management, we show that by harnessing notions from quasi-parity-time (PT) symmetry system[31], dynamically tunable single-mode laser can be readily realized in size-mismatched UCNCs-based PM (d = ~ 100 μm, t = ~ 300 nm, inset of Fig. 3a) device by asymmetric pumping and external excitation modulation. Such a kind of PM structure was proceeded through standard photolithography, followed by a second spin-coating round using a polymer compound containing UCNCs (6.5 wt%). Due to the mature CMOS technique, the size and shape of each microdisk can be well repeated in the system of two adjacent circular cavities, except for slight size-mismatching effect arising from fabrication inaccuracies of photolithography technique. Here, we define such PM laser as two tangent microdisks with similar radii of each component under asymmetric excitation, which can be experimentally realized through selectively pumping at only one constituent resonator by a NIR pulsed laser.

As shown in Fig. 3a under 808 nm right pumping, a broad luminescence at around 646 nm (i.e., $^5F_5 \rightarrow {}^5I_8$ transition of Ho^{3+} ions) emerges at the very beginning with the full width at half-maximum (FWHM) of ~ 8 nm. With the increase of pumping fluences, the spectra become quite different. Only one peak at 646.2 nm ascends from the emission band and grows rapidly above P_a (i.e., 37.33 mJ cm^{-2}). The linewidth of the individual mode, once pumped above P_a, is less than ~ 0.07 nm, corresponding to a quality (Q)-factor of ~ 9000 (i.e., $Q = \lambda/\delta\lambda$, where λ and δλ denote the resonance peak and its FWHM respectively). Figure 3b displays the corresponding light-light curves of three characteristic peaks of Ho^{3+} ions. The integrated intensity of the resulting mode as a function of power density (red open circles in Fig. 3b) presents a clear S-curve, which unambiguously confirms the onset of single-mode lasing at 646.2 nm[16, 30, 34]. In this regard, we introduce the extinction ratio (E-ratio), defined as $10log(I_1/I_2)$ (where I_1 and I_2 are the intensity of the dominant peak and the highest side one respectively), to estimate the performance of supermode. It is observed that the corresponding E-ratio value (Fig. 3b) ascends steeply and reaches a value as high as 11 dB under 808 nm right pumping. Also, PM laser exhibits an ultraviolet single-mode operation at the wavelength of 345.6 nm (i.e., $^1I_6 \rightarrow {}^3F_4$ transition of Tm^{3+} ions) with an E-ratio exceeding 13 dB under 980 nm right pumping (Fig. 3c and 3d). Apparently, there are no obvious kinks for other competing peaks (i.e., at 487 and 542 nm of Ho^{3+} ions, and 362, 451, 476 and 648 nm of Tm^{3+} ions), which thus act as typical spontaneous emission in our selectively excited PM structure. Hence, our PM device retains a single-mode laser in a wide pumping range with a switchable wavelength from 345.6 nm to 646.2 nm.

The observed mode-switching effect can be understood with the Vernier effect[35]. Figure 4a gives the schematic design of our PM device, where a fixed dual-mode upconversion material was purposely incorporated with the proposed PM structure. Note that, two microdisks directly contact with each other without any spacing. We numerically calculated two sets of resonance with identical gain spectrum to demonstrate mode selection phenomena. In the calculation, the radius of the left resonator was fixed

while that of the right one varied in order to change the size deviation of two coupled microdisks. Following the Vernier effect, once PM is activated under NIR right excitation, most of the modes leak out to the passive cavity through the joint area except for selected modes which satisfy the following equations: $mFSR_l = nFSR_r$ (i.e., where m and n should be integers). The threshold of resulting high-Q supermodes will be significantly decreased than their neighboring mode pairs. In principle, as the FSR of the multiple modes being enlarged, single-mode lasing would happen when there is only one mode emerging from the gain region of resonant peak. One unique thing to consider here is that each constituent peak of multicolour spectrum shares different FSRs and narrow linewidth owing to the intrinsic property of Ln^{3+} ions with plentiful energy states. Thus, together with two groups of distinct FSRs, only enhanced amplification of overlapped modes at 646.2 nm and 345.6 nm could be observed from our NIR right-pumped PM structure while other unwanted modes are remarkably reduced. Under the guidance of this principle, incorporated with specific sensitizer-pair and activator ions (i.e., 646 nm of Ho^{3+}, and 346 nm of Tm^{3+}), the proposed UCNCs exhibit two distinct $Nd^{3+}\rightarrow Yb^{3+}\rightarrow Ho^{3+}$ and $Yb^{3+}\rightarrow Tm^{3+}$ energy transfer paths, which can be effectively activated by 808 nm and 980 nm laser respectively. By virtue of material design, one of two mutually exclusive emitting peaks at the wavelengths of 646 nm and 346 nm would emerge from the dual-mode spectra. Controlled in a switch-like manner, our UCNCs-doped PM device would give an outstanding mode-switching performance.

A more rigorous analysis was conducted by systematically investigating the lasing actions in our PM device under three types of configuration including left pumping, right pumping, and uniform pumping (Figure S7). The corresponding simulated field distribution patterns are illustrated in the insets of Figure S8a. Figure S8a and S8c give the normalized lasing spectra above P_a under three types of pumping configurations with the corresponding light-light curves in Figure S8b and S8d, respectively. There is a slight deviation in wavelengths (Figure S9) of selected modes between left excited PM and right excited one. More interestingly, compared with our PM device under NIR left pumping, the threshold value under right pumping is lower even though two adjacent microdisks share nearly identical size and UCNCs-doping concentration (Figure S8b and S8d). Both results confirm the size gap between two coupled microdisks. Nonetheless, observation of control data (Figure S9) bolsters this narrative: the recorded spectra exhibit stable single-mode lasing emission while only one of the constituent resonators being excited, whereas it shows multimode lasing in uniformly pumped PM. It is very important to note, however, that even our UCNCs were designed with a particular emission profile, weak spontaneous emission at wavelength away from the design still emerges from such selectively excited PM. This is understandable since there is an overlap of signals owing to selected modes from right pumping and left pumping, as well as the particular modes emerging from the coincidence of the resonance between left and right resonators under uniform pumping. In principle, the PM under asymmetric excitation would hold more loss when compared to that under uniform pumping. However the threshold values of single-mode laser in our PM device, reading as 33.27 mJ cm^{-2}@347.2 nm and 37.33 mJ cm^{-2}@647.0 nm respectively, are obviously lower than that of microdisk lasers (i.e., 47.02 mJ cm^{-2}@346.6 nm, and 45.28 mJ cm^{-2}@646.2 nm), largely owing to the highly suppressed neighboring modes. The corresponding

incident energy from these competing modes would directly contribute to the improvement of resulting supermodes.

A further investigation on the uniformity and stabilization of these supermodes was performed in the short-listed PM array (inset of Fig. 5). Despite fabrication fluctuation in cavity size, a clear mode-switching phenomenon can be observed in all those neighboring PMs (Fig. 5a and b), except for slight variance in wavelengths of selected modes and the corresponding thresholds (Fig. 5c and d). Also, from the repetitive emission switching by excitation cycling between 980 nm and 808 nm in Fig. 5e, this PM laser switch shows excellent stability even though with a certain amount of intensity distinctions of supermodes. Furthermore, this PM structure can be rotated to attain the far-field pattern (Figure S11), which quantitatively reveals that our single-mode laser emitted along the direction of ΦFF = 180° with the divergence angle at around 30° under NIR right pumping. Such unidirectional emission directly results from the collimation of the unexcited cavity[31]. This situation is generally different in two structurally identical resonators, in which exact PT breaking of gain and loss symmetry only happens at an exceptional point to maximize emitting power of the specific mode without directional outputs [36–37]. Obviously, this unidirectional single-mode laser favors the subsequent integration in on-chip photonic circuits at the corresponding direction, showing remarkable potential in the field of integrated optics. All these results present a compelling evidence that our proposed strategy shows great advantages in pursuing switchable unidirectional single-mode lasing in submillimeter cavities with high tolerance in fabrication deviation and low demand in design complexity.

Discussion

In summary, these findings demonstrated that our UCNCs-based size-mismatched PM structure, even with the cavity size in submillimeter scale, holds the promise for unidirectional single-mode operation under asymmetric pumping from inherently multicolour multimode microdisk lasing, which can hardly be addressed by chemical modification or remote manipulation approaches. Such light modulation, including mode-selection, wavelength-switching, and emitting direction, is accomplished through the favorable interactions between gain and passive cavity in terms of Vernier effect accompanying with two distinct sets of FSRs between two coupled microdisks of different radii. Clearly, a large number of competing modes fall along with the amplification of selected modes in this homogeneous PM device, resulting in an enhanced single-mode laser with a high contrast ratio up to 11 dB. Particularly, this PM structure presents remarkable mode-switching functionality with high uniformity and long-term stability under external excitation modulation. The key idea behind this arrangement lies in the cavity design and inversely designed UCNCs, enabling spectral tuning of UCNCs-based PM compatible with the conventional CMOS technique, that is essential for high throughput device. Hence, we believe this strategy raises new possibilities for UCNCs to complement or extend their applications from imaging to integrated photonic circuits.

Materials And Methods

Nanoparticle synthesis. The multishelled $NaGdF_4$:Yb/Nd@$NaGdF_4$:Yb/Ho@$NaYF_4$:Ca@ $NaYbF_4$:Tm@$NaYF_4$:Ca nanocrystals were synthesized in the previously reported ref. 16. Detailed fabrication and characterization are provided in the Supplementary Information.

Device fabrication and characterization. Both of the proposed UCNCs-based microdisk laser and UCNCs-based size-mismatched photonic molecule microlaser were fabricated through tailoring the substrate[30, 34]. The proposed UCNCs-on-SiO_2 microdisk array was fabricated through a combination of standard photolithography process (SVC model H94-25C) and subsequent spin-coating operation. A group of UCNCs-based microcavities with a thickness of ~ 300 nm can be formed and characterized under the excitation of a tunable laser system consisting of a 355 nm Q-switched Nd:YAG laser (Continuum, Surelite II-10) and an optical parametric oscillator (Continuum, Horizon I). The emission spectra were collected from the boundary of such photonic device by an optical fiber coupled to the iHR-320 (Horiba) monochromator (attached with a photomultiplier tube), using 808 or 980 nm pulsed lasers (6ns, 10Hz, Φ8mm) as the pumping sources.

Declarations

Acknowledgments This work was supported by the NSFC(no. 61805058), NSFC of Guangdong Province of China(no. 2018A030310034), Shenzhen Fundamental Research Fund (no.JCYJ20180306171700036, JCYJ20190806143813064).

The authors also acknowledge support from the Shenzhen Engineering Laboratory on Organic-Inorganic Perovskite Devices, Shenzhen Scientific Research Foundation for the introduction of talent, and NSFC(no. 51802198) from Shenzhen University.

Author contributions L. J. conceived and supervised the optical experiments and analyzed the data. X.C. and H. S. designed and fabricated the luminescent materials. L. J. and X.C. wrote the paper. Y.W., X. Yangand L.J. fabricated the device and performed the optical characterization. X.C., L.J., Q.S. and S.X. contributed to analyzing and preparing this manuscript. Y. W., X.C. and L.J. contributed equally to this work.

Competing interests The authors declare no competing interests.

References

1. Huang, M. H. *et al*. Room-temperature ultraviolet nanowire nanolasers. *Science* **292**, 1897 – 1899 (2011).
2. Piccione, B., Cho, C. H., van Vugt, L. K. & Agarwal, R. All-optical active switching in individual semiconductor nanowires. *Nat. Nanotechnol.* **7**, 640–645 (2012).
3. Fan, F., Turkdogan, S., Liu, Z., Shelhammer, D. & Ning, C. Z. A monolithic white laser. *Nat. Nanotechnol.* **10**, 796–803 (2015).

4. Zhou, B., Shi, B., Jin, D. & Liu, X. Controlling upconversion nanocrystals for emerging applications. *Nat. Nanotechnol.* **10**, 924–936 (2015).
5. Wang, F. *et al*. Simultaneous phase and size control of upconversion nanocrystals through lanthanide doping. *Nature* **463**, 1061–1065 (2010).
6. Wang, F. & Liu, X. Upconversion multicolor fine-tuning: visible to near-infrared emission from lanthanide-doped $NaYF_4$ nanoparticles. *J. Am. Chem. Soc.* **130**, 5642–5643 (2008).
7. Wang, F. *et al*. Tuning upconversion through energy migration in core-shell nanoparticles. *Nat. Mater.* **10**, 968–973 (2011).
8. Zhou, B. *et al*. NIR II-responsive photon upconversion through energy migration in an ytterbium sublattice. *Nat. Photon.* **14**, 760–766 (2020).
9. Zhou, B. *et al*. Probing energy migration through precise control of interfacial energy transfer in nanostructure. *Adv. Mater.* **31**, e1806308 (2019).
10. Wang, J. *et al*. Enhancing multiphoton upconversion through energy clustering at sublattice level. *Nat. Mater.* **13**, 157–162 (2014).
11. Su, Q. *et al*. The effect of surface coating on energy migration-mediated upconversion. *J. Am. Chem. Soc.* **134**, 20849–20857 (2012).
12. Chen, D. *et al.* Lanthanide activator doped $NaYb_{1-x}Gd_xF_4$ nanocrystals with tunable down-, up-conversion luminescence and paramagnetic properties. *J. Mater. Chem.* **21**, 6186 (2011).
13. Lei, Z. *et al.* An excitation navigating energy migration of lanthanide ions in upconversion nanoparticles. *Adv. Mater.* **32**, e1906225 (2020).
14. Wen, H. *et al*. Upconverting near-infrared light through energy management in core-shell-shell nanoparticles. *Angew. Chem. Int. Ed.* **52**, 13419–13423 (2013).
15. Deng, R. *et al.* Temporal full-colour tuning through non-steady-state upconversion. *Nat. Nanotechnol.* **10**, 237–242 (2015).
16. Chen, X. *et al.* Confining energy migration in upconversion nanoparticles towards deep ultraviolet lasing. *Nat Commun.* **7**, 10304 (2016).
17. Zhao, J. *et al*. Single-nanocrystal sensitivity achieved by enhanced upconversion luminescence. *Nat. Nanotechnol.* **8**, 729–734 (2013).
18. Zhang, C. *et al*. White-light emission from an integrated upconversion nanostructure: toward multicolor displays modulated by laser power. *Angew. Chem. Int. Ed. Engl.* 54(39): 11531–11535 (2015).
19. Lu, Y. *et al.* Tunable lifetime multiplexing using luminescent nanocrystals. *Nat. Photon.* **8**, 32–36 (2014).
20. Li, D. *et al.* Anomalous temperature-dependent upconversion luminescence of small-sized $NaYF_4:Yb^{3+}$, Er^{3+} nanoparticles. *J. Phys. Chem. C* **118**, 22807–22813 (2014).
21. Wang. Y. *et al.* Upconversion luminescence of β-$NaYF_4:Yb^{3+},Er^{3+}$@β-$NaYF_4$ core/shell nanoparticles: excitation power density and surface dependence. *J. Phys. Chem. C* **113**, 7164–7169 (2009).

22. Jia, X. *et al.* Polyacrylic acid modified upconversion nanoparticles for simultaneous pH-triggered drug delivery and release imaging. *J. Biomed. Nanotechnol.* **9**, 2063–2072 (2013).
23. Wang, C. *et al.* Imaging-guided pH-sensitive photodynamic therapy using charge reversible upconversion nanoparticles under near-infrared light. *Adv. Funct. Mater.* **23**, 3077–3086 (2013).
24. Mundoor, H. & Smalyukh, I. I. Mesostructured composite materials with electrically tunable upconverting properties. *Small* **11**, 5572–5580 (2015).
25. Liu, Y., Wang, D., Shi, J., Peng, Q. & Li, Y. Magnetic tuning of upconversion luminescence in lanthanide-doped bifunctional nanocrystals. *Angew. Chem. Int. Ed.* **52**, 4366–4369 (2013).
26. Gnidakouong, J. R. N. & Yun, G. J. Dislocation density level induced divergence between stress-free afterglow and mechanoluminescence in $SrAl_2O_4$: Eu^{2+}, Dy^{3+}. *Ceram. Int.* **45**, 1794–1802 (2019).
27. Xu, C. N., Watanabe, T., Akiyama, M. & Zheng, X. G. Direct view of stress distribution in solid by mechanoluminescence. *Appl. Phys. Lett.* **74**, 2414 – 2416 (1999).
28. Peng, D., Recent advances in doped mechanoluminescent phosphors. *ChemPlusChem* 80, 1209 (2015).
29. Zhang, C. *et al*. Dual-color single-mode lasing in axially coupled organic nanowire resonators. *Sci. Adv.* **3**, e1700225 (2017).
30. Jin, L. *et al*. Mass-manufactural lanthanide-based ultraviolet B microlasers. *Adv. Mater.* **31**, 1807079 (2019).
31. Zhang, N. *et al*. Quasi parity-time symmetric microdisk laser. *Laser Photonics Rev.* **11**, 1700052 (2017).
32. Wang, T. *et al*. White-light whispering-gallery-mode lasing from lanthanide-doped upconversion $NaYF_4$ hexagonal microrods. *ACS Photon.* **4**, 1539–1543 (2017).
33. Ma, R. M. and R. F. Oulton (2019). "Applications of nanolasers." Nat Nanotechnol **14**(1): 12–22.
34. Huang, C. *et al.* Highly Controllable Lasing Actions in Lead Halide Perovskite-Si_3N_4 Hybrid Micro-Resonators. *Laser Photonics Rev.* **13**, 1800189 (2019).
35. Li, F., et al. (2021). "Single-mode lasing of CsPbBr3 perovskite NWs enabled by the Vernier effect." Nanoscale **13**(8): 4432–4438.
36. Hodaei, H., Miri, M., Heinrich, M., Christodoulides, D. N. & Khajavikan, M. Parity-time–symmetric microring lasers. *Science* **346**, 975 (2014).
37. Peng, B. *et al*. Parity–time-symmetric whispering-gallery microcavities. *Nature Phys.* **10**, 394–398 (2014).

Figures

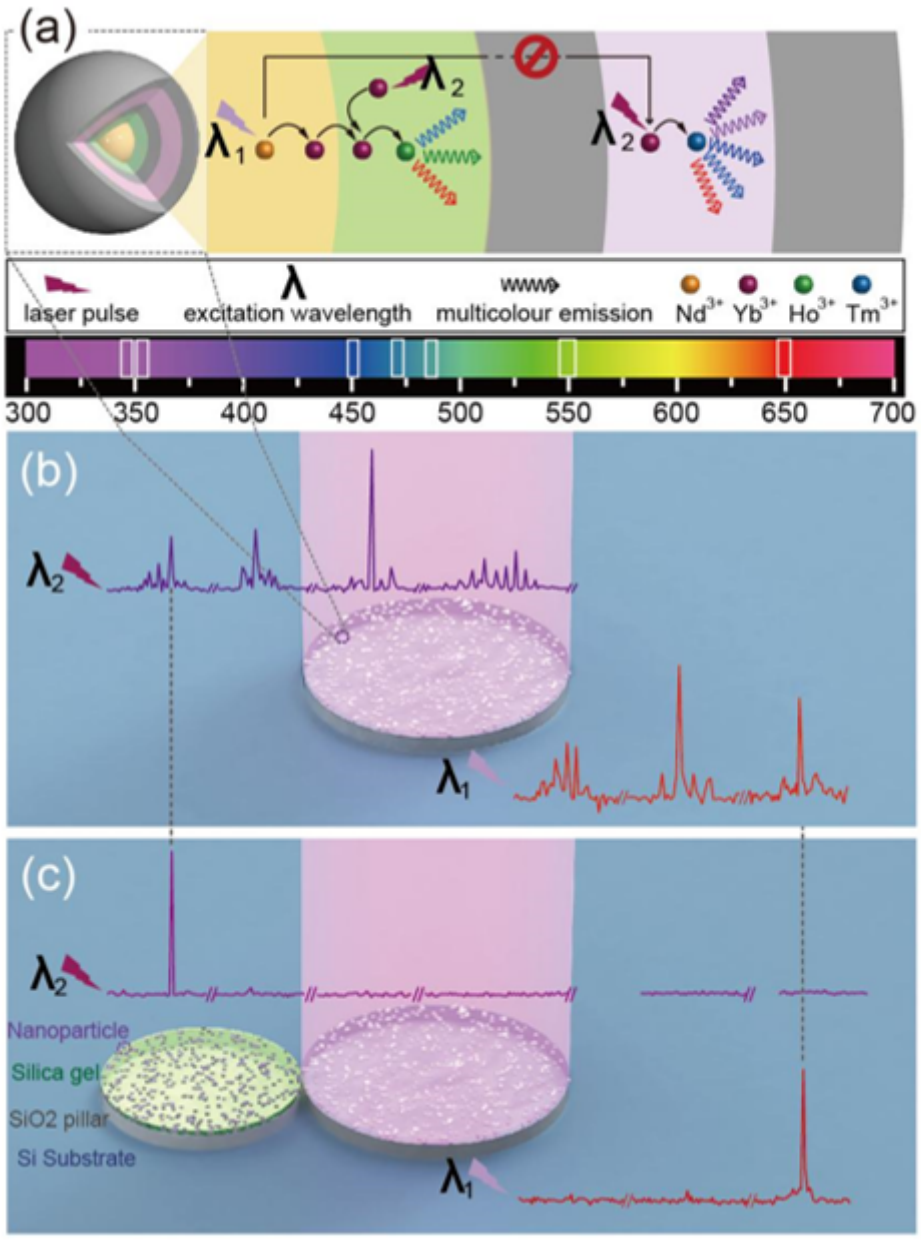

Figure 1

Principle of mode-switching concept in UCNCs-based size-mismatched PM laser. (a) Illustration of Ln3+-doped multishelled nanocrystals featured with two distinct upconverting processes upon the excitation of λ1 and λ2 lasers, respectively. (b) An isolated UCNCs-based microdisk simultaneously supports multimode lasing emission with the emission wavelengths spanning over a wide spectral range. (c) UCNCs-based size-mismatched PM is used to achieve dual-wavelength single-mode laser under λ1/λ2 pumping.

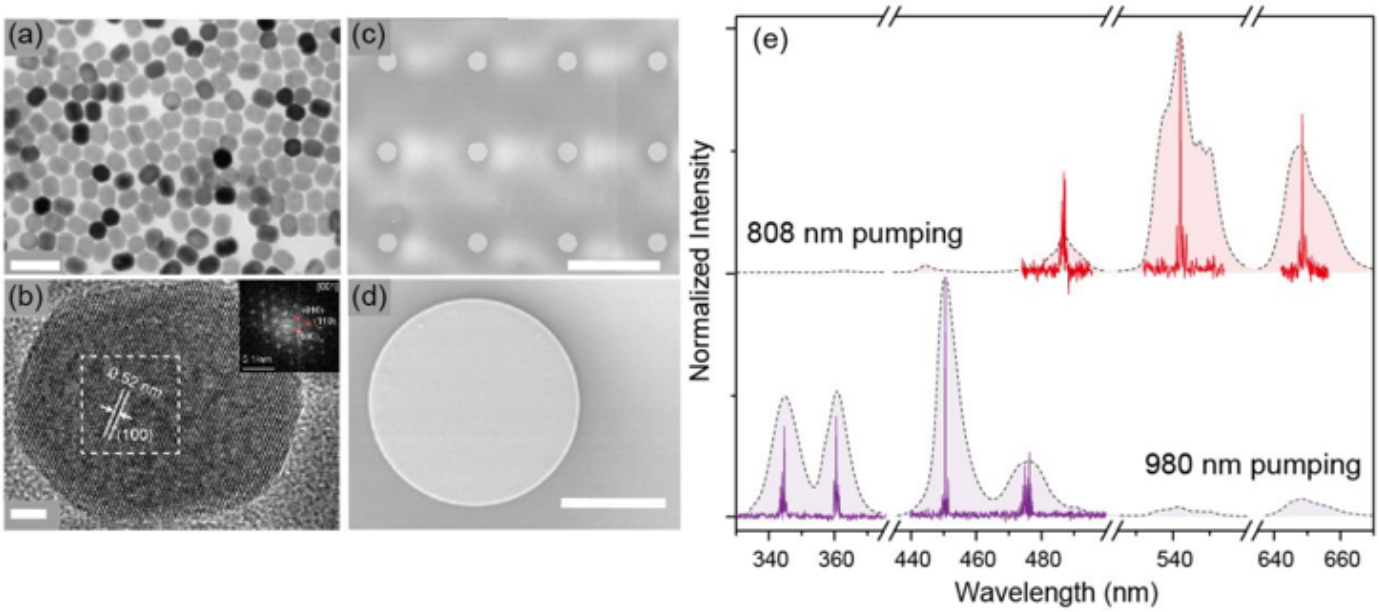

Figure 2

Realization of UCNCs-based microdisk lasers. (a) TEM and (b) High-resolution TEM images of the NaGdF4:Yb/Nd@NaGdF4:Yb/Ho@NaYF4:Ca@NaYbF4:Tm@NaYF4:Ca multishelled nanocrystal. The scale bars are 100 nm and 5 nm, respectively. Inset gives the Fourier transform diffraction pattern of the region indicated in (b). SEM images of (c) a typical set of UCNCs-based microdisk array, and (d) an isolated one with the diameter(d) of ~100 μm and thickness(t) of ~300 nm, respectively. The scale bars are 500 μm and 50 μm, respectively. (e) The observation of PL spectra (the dotted lines) from UCNCs solution under CW 808/980 nm excitation at a power of 20 W cm-2 respectively, and multimode WGMs lasing emission (the solid red/violet lines) from single microdisk in figure (d) pumped by 808/980 nm pulsed lasers at a power of 93 mJ cm-2, respectively.

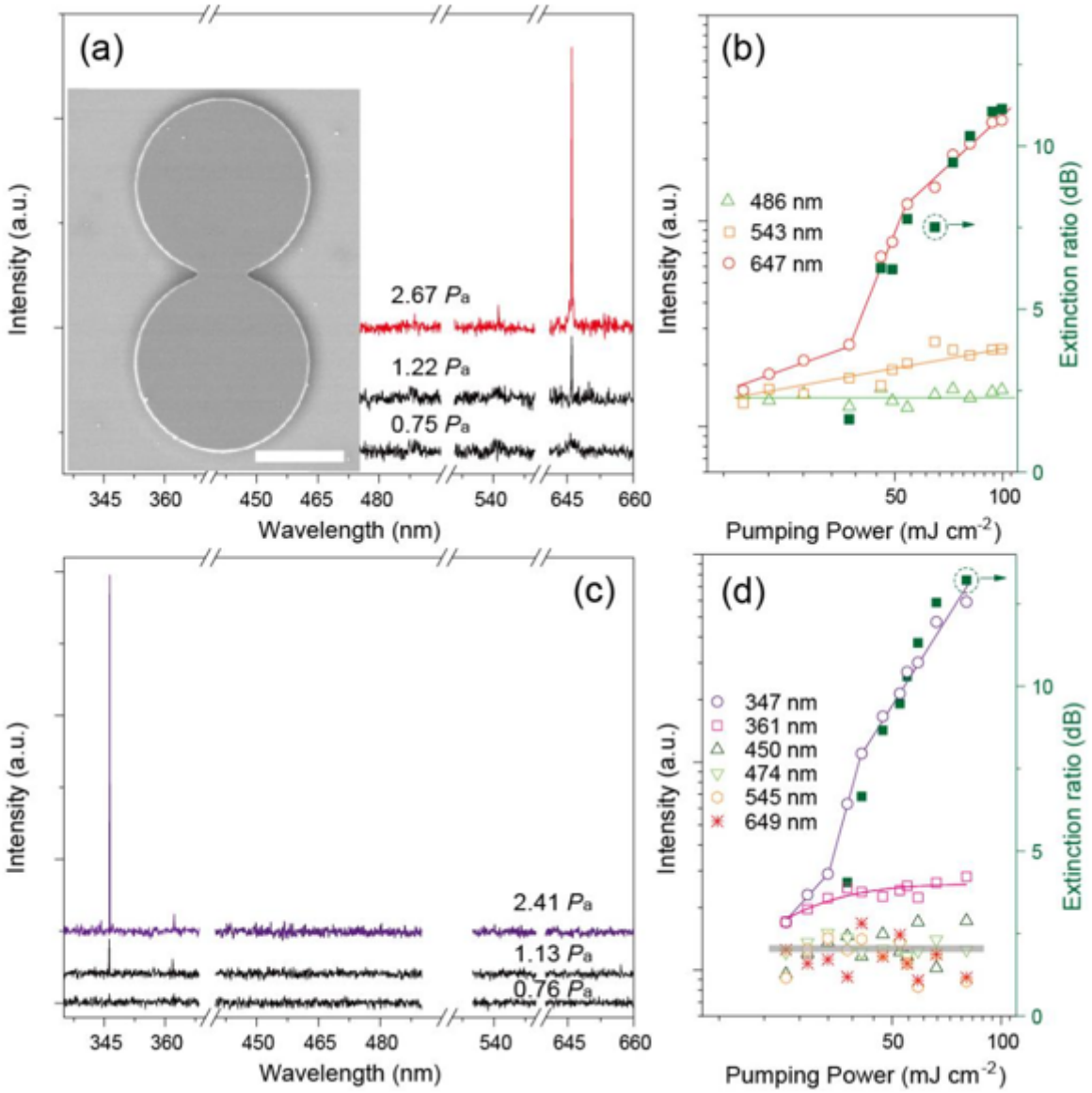

Figure 3

Realization of single-mode laser in UCNCs-based size-mismatched PM device. The emission spectra of PM structure under (a) 808 nm, and (c) 980 nm right pumping, respectively. The inset gives the SEM image of an individual PM structure with the scale bar of 50 μm. (b, d) Characteristic light-light curves of the typical peaks in figure (a, c), respectively. The filled green boxes represent the E-ratio. Solid lines are linear fittings to guide the eyes.

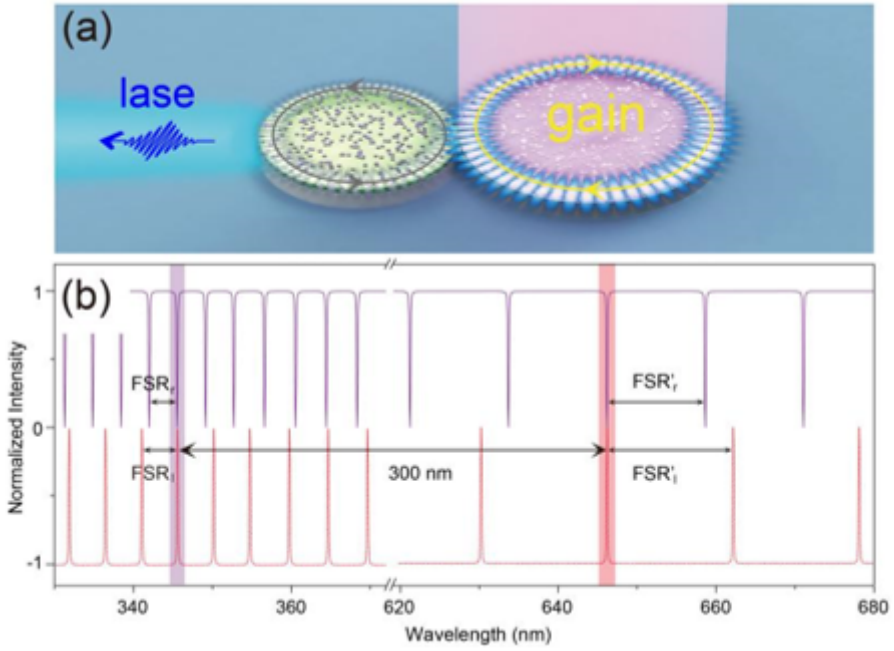

Figure 4

Theoretical calculation of mode-switching mechanism in UCNCs-based size-mismatched PM structure. (a) Schematic illustration of the PM structure, and (b) calculation of mode-selection concept.

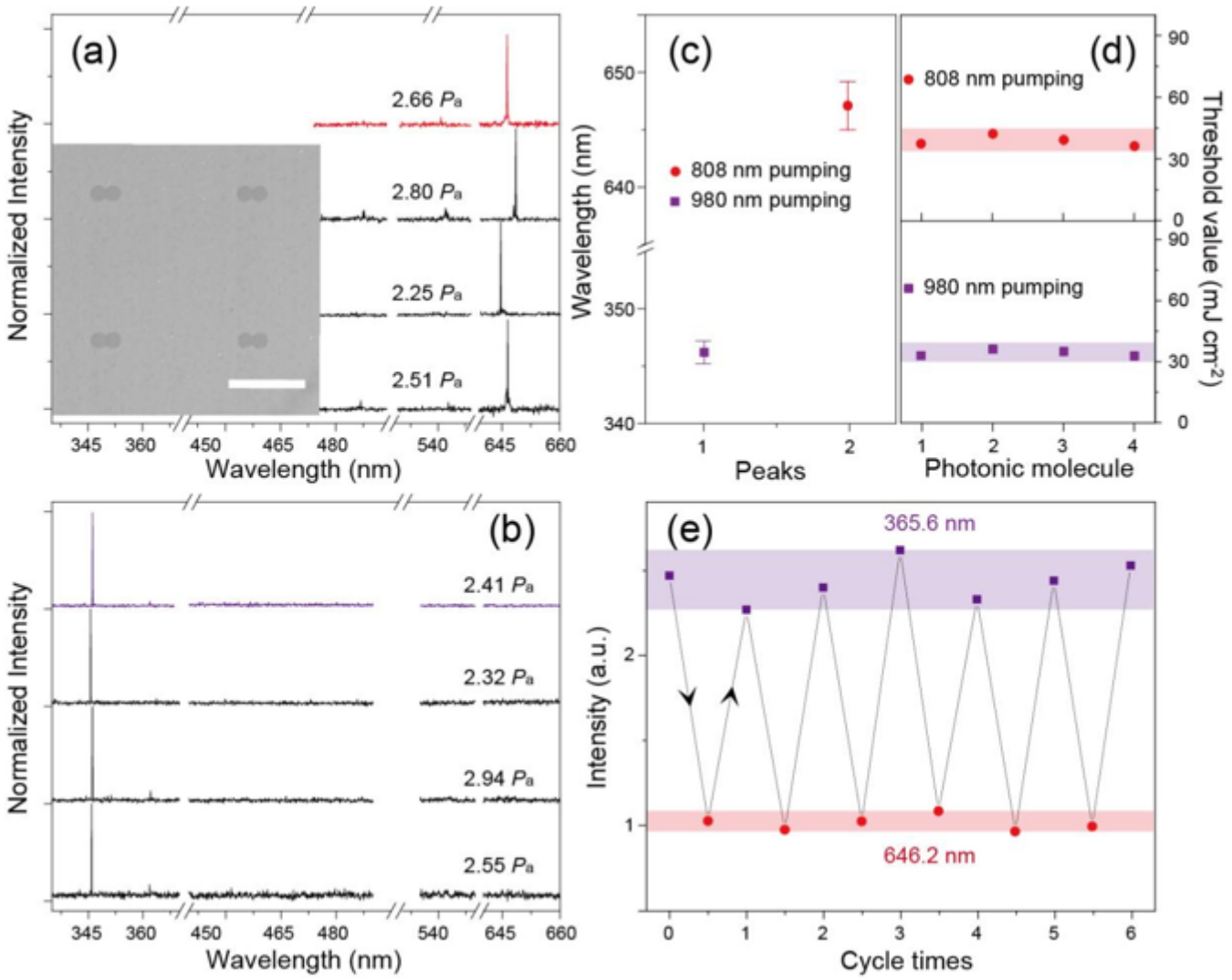

Figure 5

The uniformity of UCNCs-based PM laser. Normalized emission spectra of the short-listed PM devices under (a) 808 nm, and (b) 980 nm right pumping, respectively. The inset shows the SEM image of PM array with the scale bar of 500 μm. The statistical deviation in (c) wavelengths, and (d) thresholds of single-mode laser in (a,b), respectively. (e) Plot of the emission intensity of 365.6 nm and 646.2 nm against the 980 nm - 808 nm excitation cycles from the right excited PM laser.

Supplementary Files

This is a list of supplementary files associated with this preprint. Click to download.

- SI.docx